Supporting Information

Espinar et al. 10.1073/pnas.1216091110

SI Materials and Methods

Growth Conditions for Microscopy. For the experiments presented in the main text, *Bacillus subtilis* cells were grown at 37 °C in Luria Broth (Miller's modification) (LB) with appropriate antibiotics for selection, added to the following final concentrations: 10 μg/mL spectinomycin, 5 μg/mL chloramphenicol, 5 μg/mL kanamycin, and 5 μg/mL erythromycin. Cells were grown to an OD of 1.8 and resuspended in 0.5 vol of resuspension media (RM) (composition per 1 L: 0.046 mg of $FeCl_2$, 4.8 g of $MgSO_4$, 12.6 mg of $MnCl_2$, 535 mg of NH_4Cl, 106 mg of Na_2SO_4, 68 mg of KH_2PO_4, 96.5 mg of NH_4NO_3, 219 mg of $CaCl_2$, 2 g of L-glutamic acid) (1). The cells were incubated at 37 °C for 1.5 h, then diluted 10-fold in RM and applied onto a 1.5% (wt/vol) low-melting agarose pad placed into a coverslip-bottom Willco dish for imaging. When necessary, the cultures and agarose pads were adjusted to the final isopropyl β-D-1-thiogalactopyranoside (IPTG) concentrations of 3, 5, 10, and 100 μM. *B. subtilis* microcolonies in the pads were imaged with fluorescence time-lapse microscopy at 37 °C with a Nikon TE2000 inverted microscope and a motorized stage (Prior). Images were acquired every 20 min with a Hamamatsu ORCA-ER camera. Imaging time was optimized to prevent phototoxicity (2). The NIS-Elements software was used to automate image acquisition and microscope control. Data analysis of time-lapse movies was performed by custom software developed with MATLAB image processing and statistics toolboxes (MathWorks).

For the general stress experiments shown in Fig. S3 below, *B. subtilis* cells were grown overnight at 30 °C in LB without antibiotics. Then, cells were diluted to an OD of 0.1 into 10 mL of LB (1:20) in PBS and incubated at 37 °C for a period ranging from 4 to 6 h. Finally, cells were diluted to a final OD = 0.1–0.12 and placed into a 2% (wt/vol) low-melting agarose pad made of conditioned medium (1:30; prepared as described below) in PBS enriched with L-glutamate at a final concentration of 0.21% (wt/vol). When necessary, IPTG was added to cultures and agarose pads at a final concentration of 5 μM. Conditioned media was prepared growing PY79 wild-type *B. subtilis* strain in 2 mL of LB at 37 °C for 4.5 h. Then, this culture was diluted in 23 mL of fresh LB and was grown at 37 °C for 17.5 h. After this, cells were removed by centrifugation (at 3,000 × *g* for 10 min) and the supernatant was sterilized by filtration (using 0.2-μm pore-size filters) and stored at −80 °C. This is a variation of the conditioned media used in previous works (3, 4).

Strain Construction. The strains 75xS and Control-βS-75xS were constructed from the plasmid pDG148 (kind gift from Beth A. Lazazzera, University of California, Los Angeles, CA). PCR was used to amplify native P_{comS}-*comS* and P_{comS}-*cfp* fusion constructs. The amplified constructs were cloned into pDG148 using EcoRV and BamHI restriction sites. We then transformed these plasmids into the strains containing chromosomally integrated P_{comG}-*cfp* and P_{comS}-*yfp* reporters (V10) and P_{hyp}-*yfp* (Control-α).

For the construction of the Control-βS-6xS strain, we used the low-copy number plasmid pHP13 (5). PCR was used to amplify a P_{comS}-*cfp* fusion constructs. The resulting construct was cloned into pHP13 using SmaI and BamHI restriction sites. We then transformed this plasmid into the strain containing chromosomally integrated P_{hyp}-*yfp* (Control-α).

The strain Norm-βS was obtained by transformation of the pDL30 plasmid (kind gift from Jonathan Dworkin, Columbia University, New York, NY), designed to integrate into the *amyE* locus and carrying the construct P_{comS}-*cfp*.

The Hyper-αS-6xS and Hyper-αS-75xS strains were obtained by transformation of the pHP13::P_{comS}-*comS* and pDG148::P_{comS}-*comS* plasmids, respectively, into the Hyper-αS strain. In the same way, the Hyper-αK-6xS and Hyper-αK-75xS strains were obtained by transformation of the plasmids pHP13::P_{comS}-*comS* and pDG148::P_{comS}-*comS*, respectively, into the Hyper-αK strain.

Dose–Response and Calibration of P_{hyp} Activity. To calibrate the expression of the IPTG-inducible hyperspank promoter (P_{hyp}) used in the Hyper-αS, Hyper-αS-6xS, Hyper-αS-75xS, Hyper-αK, Hyper-αK-6xS, and Hyper-αK-75xS strains, we measured P_{hyp}-*yfp* fluorescence levels in the Control-α strain. Cells were grown on 1.5% (wt/vol) low melting agarose pads made with resuspension medium (RM) and final IPTG concentrations of 0, 3, 5, 10, and 100 μM. The dose–response curve of P_{hyp}-*yfp* as a function of IPTG is shown in Fig. S1. Alongside P_{hyp}-*yfp* expression levels at various IPTG concentrations, we simultaneously measured the activity of P_{comK}-*yfp* using the KG strain, and of P_{comS}-*yfp* using the V10 strain. This allowed us to calibrate P_{hyp}-*yfp* activity in units of α_k^{wt} and β_s^{wt} activity, respectively, in noncompetent cells. Table S2 shows a summary of the control data at 0, 3, 5, 10, and 100 μM IPTG concentration.

Calibration of P_{comS} Promoter Activity Triggered by Plasmids. To calibrate the expression of P_{comS}-*comS* triggered by the plasmids pHP13::P_{comS}-*comS* and pDG148::P_{comS}-*comS*, we constructed the pHP13::P_{comS}-*cfp* and pDG148::P_{comS}-*cfp* plasmids, respectively (see *Strain Construction* for strain construction and Table S1 for strain genotype). To normalize the expression levels of these strains to the wild-type *comS* expression, we constructed the Norm-βS strain, carrying P_{comS}-*cfp* integrated into the *amyE* locus. We simultaneously measured *cfp* levels in these strains using time-lapse microscopy, and normalized the data dividing time-to-time the fluorescence obtained in the pHP13::P_{comS}-*cfp* and pDG148::P_{comS}-*cfp* by that from P_{comS}-*cfp* in the Norm-βS strain. Fig. S2 shows in black and red (continuous line) the resulting traces obtained from the Control-βS6xS and Control-βS75xS strains, respectively. The dashed lines represent the stationary value of the normalized time traces.

Determination of the Probabilities of Initiation, Exit, and Reinitiation. The probability of competence initiation (P_{init}) was determined as follows. Under conditions that allow initiation of competence (see *Strain Construction*), P_{init} was defined as the number of competence initiation events divided by the total number of cell division events in a time window of ∼140–150 min, characterized by increasing levels of P_{comS}-*yfp* (which ensures that the colony is under sustained growth conditions). The probability of competence exit (P_{exit}) was calculated as the fraction of competent cells that successfully leave the competence state. Finally, the probability of reinitiation P_{reini} is defined as the probability that a cell, after coming out of competence, goes back into that state after a fixed amount of time, in our case taken to be equal to two cell cycles. Tables S3–S5 present a summary of the statistics leading to the three probabilities measured experimentally for all input conditions.

Discrete Simulations of the Competence Circuit. The competence circuit was simulated by means of stochastic simulations using Gillespie's first reaction method (6). The simulated biochemical reactions are as follows:

$$P_{comK}^{\text{const}} \xrightarrow{k_1} P_{comK}^{\text{const}} + \text{mRNA}_{comK}$$
$$P_{comK} \xrightarrow{f(K,k_2,k_k,n)} P_{comK} + \text{mRNA}_{comK}$$
$$\text{mRNA}_{comK} \xrightarrow{k_3} \text{mRNA}_{comK} + \text{ComK}$$
$$P_{comS}^{\text{const}} \xrightarrow{k_4} P_{comS}^{\text{const}} + \text{mRNA}_{comS}$$
$$P_{comS} \xrightarrow{g(K,k_5,k_s,p)} P_{comS} + \text{mRNA}_{comS}$$
$$\text{mRNA}_{comS} \xrightarrow{k_6} \text{mRNA}_{comS} + \text{ComS}$$
$$\text{mRNA}_{comK} \xrightarrow{k_7} \emptyset$$
$$\text{ComK} \xrightarrow{k_8} \emptyset$$
$$\text{mRNA}_{comS} \xrightarrow{k_9} \emptyset$$
$$\text{ComS} \xrightarrow{k_{10}} \emptyset$$
$$\text{MecA} + \text{ComK} \underset{k_{-11}}{\overset{k_{11}/\Omega}{\rightleftharpoons}} \text{MecA}_{\text{K}}$$
$$\text{MecA}_{\text{K}} \xrightarrow{k_{12}} \text{MecA}$$
$$\text{MecA} + \text{ComS} \underset{k_{-13}}{\overset{k_{13}/\Omega}{\rightleftharpoons}} \text{MecA}_{\text{S}}$$
$$\text{MecA}_{\text{S}} \xrightarrow{k_{14}} \text{MecA},$$

where P_i^{const} and P_i are the constitutive and regulated promoters of their corresponding genes, k_i are the reaction rates, and Ω represents a volume factor, which we take to be equal to 1 molecule/nM (7). The transcriptional regulation of ComK and ComS is represented by the following Hill functions:

$$f(K,k_2,k_k,n) = \frac{k_2(K/\Omega)^n}{k_k^n + (K/\Omega)^n}, \quad g(K,k_5,k_s,p) = \frac{k_5}{1+(K/(\Omega k_s))^p},$$

where K and S are the number of ComK and ComS molecules, respectively, and k_k (k_s) represent the concentration of ComK for which the activation of ComK (repression of ComS) is half-maximal. The number of MecA molecules is conserved; here, we assumed it to be equal to 1,000 molecules. The values of the reaction rates, which are compatible with the values of the parameters of the deterministic model according to the conversion rules given in ref. 7, are listed in Table S6.

One can ask whether the good agreement between experiment and theory exhibited in Fig. 4 depends on the criteria used to classify the dynamical behavior from the experimentally measured probabilities. The criteria used in this case are defined in the caption of that figure. Modifications of these criteria do not change the results qualitatively, although they certainly affect some of the dynamical assignments, especially those close to the theoretical bifurcation lines. This is to be expected, because due to the existence of underlying biochemical noise, the boundaries defined by the bifurcation lines are smoothed out. To assess the importance of this effect, we performed discrete simulations of the reactions listed above. The grayscale color maps in Fig. 4 represent the simulated values of the three event probabilities defined above: P_{init} in Fig. 4 *A* and *D*, P_{exit} in Fig. 4 *B* and *E*, and P_{reini} in Fig. 4 *C* and *F*. The results show that in the presence of noise the deterministically predicted transitions are robust, whereas the probabilities vary smoothly across the deterministic bifurcation lines. Modifying the probability threshold values given in the caption of Fig. 4 would change the way a simulation result is classified within one dynamical regime or another, similarly to what happens with the experimental results. These changes, however, do not alter the qualitative conclusions that can be extracted from the theoretical model, which provide an explanation for the distinct integration responses of the circuit to different input pairs, in terms of the diverse bifurcation scenarios triggered by the various inputs.

1. Sterlini JM, Mandelstam J (1969) Commitment to sporulation in Bacillus subtilis and its relationship to development of actinomycin resistance. *Biochem J* 113(1):29–37.
2. Süel GM, Garcia-Ojalvo J, Liberman LM, Elowitz MB (2006) An excitable gene regulatory circuit induces transient cellular differentiation. *Nature* 440(7083): 545–550.
3. Cağatay T, Turcotte M, Elowitz MB, Garcia-Ojalvo J, Süel GM (2009) Architecture-dependent noise discriminates functionally analogous differentiation circuits. *Cell* 139(3):512–522.
4. Locke JCW, Young JW, Fontes M, Hernández Jiménez MJ, Elowitz MB (2011) Stochastic pulse regulation in bacterial stress response. *Science* 334(6054):366–369.
5. Haima P, Bron S, Venema G (1987) The effect of restriction on shotgun cloning and plasmid stability in Bacillus subtilis Marburg. *Mol Gen Genet* 209(2):335–342.
6. Gillespie DT (1977) Exact stochastic simulation of coupled chemical reactions. *J Phys Chem* 81:2340.
7. Süel GM, Kulkarni RP, Dworkin J, Garcia-Ojalvo J, Elowitz MB (2007) Tunability and noise dependence in differentiation dynamics. *Science* 315(5819):1716–1719.

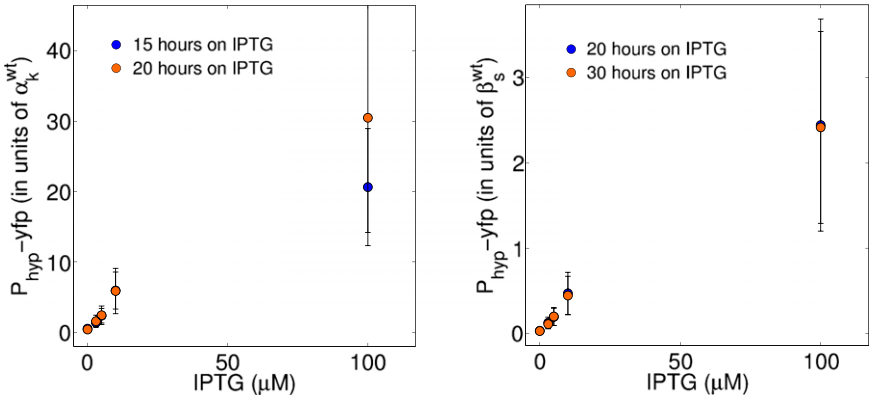

Fig. S1. Dose–response of P_{hyp}-*yfp* to IPTG. The plots show P_{hyp}-*yfp* levels as a function of IPTG concentration. Fluorescence levels were measured at 15 and 20 h of growth on IPTG pads for P_{comK}-*yfp* calibration (left plot), and at 20 and 30 h of growth on IPTG pads for P_{comS}-*yfp* calibration (right plot).

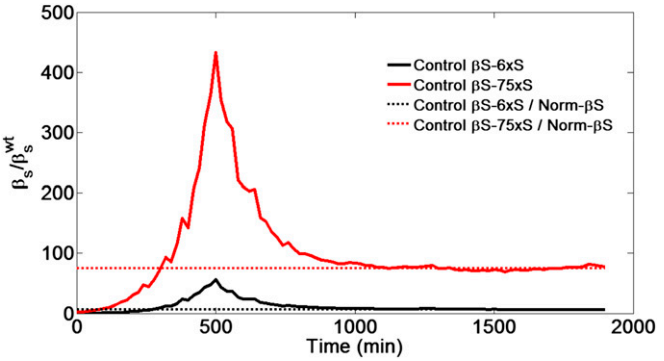

Fig. S2. Calibration of P_{comS} promoter activity. Continuous lines represent the normalized time traces obtained by dividing the mean fluorescence of the Control-βS-6xS (n = 10, black) and Control-βS-75xS (n = 15, red), by that of the single-copy strain Norm-βS (n = 10). The dashed lines represent the mean stationary values of these normalized traces, which are 6.46 and 74.97 for the pHP13::P_{comS}-*cfp* and pDG148::P_{comS}-*cfp* plasmids, respectively.

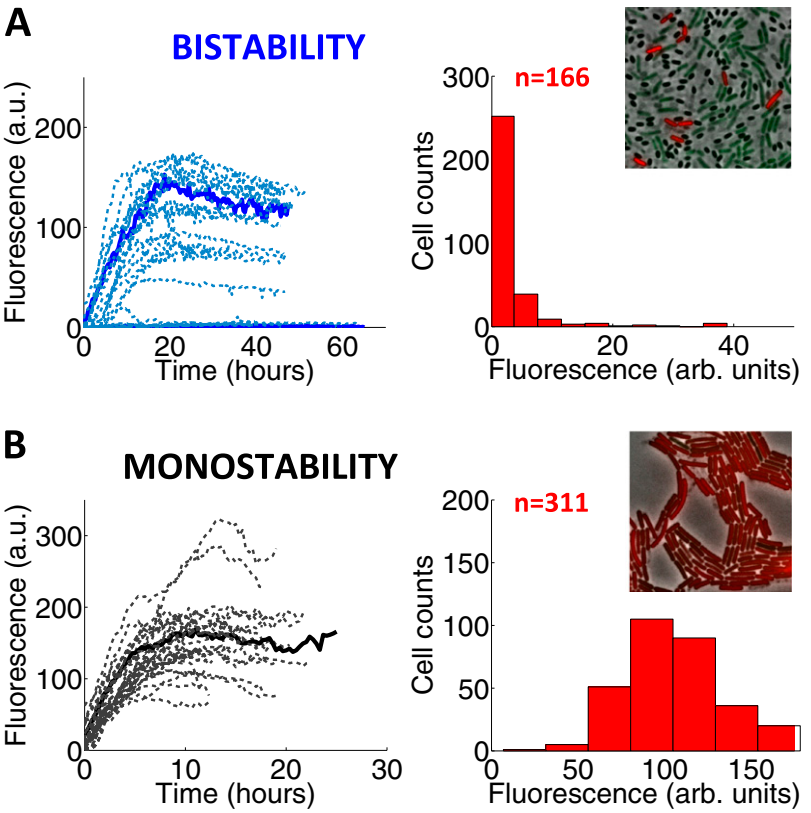

Fig. S3. Dynamical phenotypes arising from an increase in general stress signals. The figure shows the single-cell dynamics when the bacteria are grown in conditioned media (see *SI Materials and Methods, Growth Conditions for Microscopy*, for details), for the wild-type strain V10 (Table S1) in *A*, and for the Hyper-αK strain with an intermediate level of IPTG in *B*. Specifically, in *A*, $\alpha_k/\alpha_k^{wt} = 1$, and in *B*, $\alpha_k/\alpha_k^{wt} = 3.2$, corresponding to Fig. 5 *E* and *F*, but using here real stress conditions instead of an increase in ComS copy number. In each panel, the left plot shows single-cell time traces of CFP levels quantifying P_{comG} activity, with a particular time trace highlighted with a thicker line, and the right plot presents histograms of CFP levels as measured from a typical frame in each movie analyzed (at an intermediate time, because at large times there is substantial death and sporulation in the system). *Insets* display selected snapshots from these movies.

Table S1. Strains used in this study, including genotype definition and source

Strain name	Genotype	Source
V10	*AmyE*::P_{ComG}-*cfp*-P_{ComS}-*yfp*	Ref. 1
6xS	*AmyE*::P_{ComG}-*cfp*-P_{ComS}-*yfp* pHP13::P_{ComS}-*comS*	Ref. 2
75xS	*AmyE*::P_{ComG}-*cfp*-P_{ComS}-*yfp* pDG148::P_{ComS}-*comS*	This study
Hyper-αS	*AmyE*::P_{hyp}-*comS* *SacA*::P_{ComG}-*cfp*-P_{ComS}-*yfp*	Ref. 2
Hyper-αS-6xS	*AmyE*::P_{hyp}-*comS* *SacA*::P_{ComG}-*cfp*P_{ComS}-*yfp* pHP13::P_{ComS}-*comS*	This study
Hyper-αS-75xS	*AmyE*::P_{hyp}-*comS* *SacA*::P_{ComG}-*cfp*P_{ComS}-*yfp* pDG148::P_{ComS}-*comS*	This study
Hyper-αK	*AmyE*::P_{hyp}-*comK* *SacA*::P_{ComG}-*cfp*P_{ComS}-*yfp*	This study
Hyper-αK-6xS	*AmyE*::P_{hyp}-*comK* *SacA*::P_{ComG}-*cfp*P_{ComS}-*yfp* pHP13::P_{ComS}-*comS*	This study
Hyper-αK-75xS	*AmyE*::P_{hyp}-*comK* *SacA*::P_{ComG}-*cfp*P_{ComS}-*yfp* pDG148::P_{ComS}-*comS*	This study
KG	*AmyE*::P_{ComG}-*cfp*-P_{ComK}-*yfp*	Ref. 1
Control-α	*AmyE*::P_{hyp}-*yfp*	Ref. 2
Control-βS-6xS	*AmyE*::P_{hyp}-*yfp* pHP13::P_{ComS}-*cfp*	This study
Control-βS-75xS	*AmyE*::P_{hyp}-*yfp* pDG148::P_{ComS}-*cfp*	This study
Norm-βS	*AmyE*::P_{ComS}-*cfp*	This study

1. Suel GM, Garcia-Ojalvo J, Liberman LM, Elowitz MB (2006) An excitable gene regulatory circuit induces transient cellular differentiation. *Nature* 440(7083):545–550.
2. Suel GM, Kulkarni RP, Dworkin J, Garcia-Ojalvo J, Elowitz MB (2007) Tunability and noise dependence in differentiation dynamics. *Science* 315(5819):1716–1719.

Table S2. Fluorescence of control strains at 0, 3, 5, 10, and 100 μM of IPTG concentration, at 15, 20, and 30 h

	Fluorescence of control strains, arbitrary units								
Strain name	15 h	SEM	*n*	20 h	SEM	*n*	30 h	SEM	*n*
V10	79.70	43.80	155	57.74	26.50	252	57.98	25.19	102
KG	6.12	1.99	77	4.63	2.25	52	—	—	—
Control-α 0 μM IPTG	3.14	0.87	118	1.79	0.81	107	1.56	0.79	48
Control-α 3 μM IPTG	8.32	1.94	160	7.22	1.87	251	6.27	1.70	86
Control-α 5 μM IPTG	14.39	4.34	207	11.15	2.81	131	11.44	3.47	55
Control-α 10 μM IPTG	36.31	10.98	217	27.14	6.96	203	25.69	6.82	73
Control-α 100 μM IPTG	126.30	30.14	214	141.13	31.16	250	139.93	23.25	96

n = number of cells analyzed.

Table S3. Probability of initiation for all input conditions

IPTG, μM	$\beta_s = 1$, n	Probability, %	SEM	$\beta_s = 6.5$, n	Probability, %	SEM	$\beta_s = 75$, n	Probability, %	SEM
Probability of initiation for varying α_s									
wt	11/534	2.26	0.26	38/781	4.90	0.42	243/1,485	16.86	1.35
0	12/838	1.46	0.24	16/337	4.66	0.30	126/745	16.32	1.76
3	10/637	1.52	0.13	52/591	8.45	0.53	38/231	16.53	2.00
5	14/801	1.72	0.30	54/602	8.61	0.89	94/538	18.61	1.86
10	24/592	3.61	0.72	31/213	12.91	1.81	88/431	18.94	1.27
100	71/891	8.24	1.14	94/119	16.38	1.33	84/444	21.02	0.68
Probability of initiation for varying α_k									
wt	11/534	2.26	0.26	38/781	4.90	0.42	243/1,485	16.86	1.35
0	12/388	3.37	0.39	46/243	18.05	2.17	NA	100.00	NA
3	95/546	17.39	1.56	175/329	54.36	3.67	NA	100.00	NA
5	464/695	64.95	4.03	NA	100.00	NA	NA	100.00	NA
10	131/193	67.90	2.86	NA	100.00	NA	NA	100.00	NA
100	NA	100.00	NA	NA	100.00	NA	NA	100.00	NA

n = fraction of initiation of competence events with respect to all cell division events; NA, not applicable, all cells enter in competence; wt, wild type.

Table S4. Probability of exit for all input conditions

IPTG, μM	$\beta_s = 1$, n	Probability, %	SEM	$\beta_s = 6.5$, n	Probability, %	SEM	$\beta_s = 75$, n	Probability, %	SEM
Probability of exit for varying α_s									
wt	88/147	61.12	3.41	57/122	48.77	4.86	12/287	4.12	0.32
0	21/35	61.21	5.11	51/596	44.29	6.30	14/596	2.34	0.94
3	13/25	52.80	5.53	31/123	24.84	1.79	9/365	2.32	0.30
5	27/54	48.91	5.56	76/326	23.77	1.83	7/353	1.96	0.43
10	17/76	22.24	3.21	3/59	5.13	0.13	8/660	1.20	0.23
100	17/220	8.93	3.62	25/525	4.77	0.27	4/429	0.99	0.71
Probability of exit for varying α_k									
wt	88/147	61.12	3.41	57/122	48.77	4.86	12/287	4.12	0.32
0	16/26	62.14	3.54	12/380	3.19	0.57	10/340	2.95	0.17
3	45/74	61.55	2.49	13/405	3.18	0.54	9/360	2.56	0.56
5	63/115	55.39	3.72	12/435	2.79	0.29	7/350	2.01	1.84
10	58/103	56.71	2.95	NA	0.00	NA	NA	0.00	NA
100	NA	0.00	NA	NA	0.00	NA	NA	0.00	NA

n = fraction of competent cells that successfully leave the competence state with respect to all competence events; NA, not applicable, cells do not exit competence; wt, wild type.

Table S5. Probability of reinitiation for all strains

IPTG, μM	$\beta_s = 1$, N	Probability, %	SEM	$\beta_s = 6.5$, n	Probability, %	SEM	$\beta_s = 75$, n	Probability, %	SEM
Probability of reinitiation for varying α_s									
wt	6/213	2.38	0.92	9/240	2.96	1.01	8/192	2.93	1.09
0	3/87	2.43	1.31	6/193	3.09	1.46	5/127	2.97	1.33
3	2/64	2.23	1.41	8/207	3.80	1.46	4/96	5.11	1.94
5	2/101	2.22	1.36	12/299	4.05	1.03	3/96	5.65	3.35
10	4/90	3.75	1.27	4/67	4.13	1.40	2/60	4.22	2.59
100	3/93	3.54	2.04	13/360	3.18	0.85	3/84	3.11	1.30
Probability of reinitiation for varying α_k									
wt	6/213	2.38	0.92	9/240	2.96	1.01	8/192	2.93	1.09
0	7/121	3.47	1.58	2/66	3.06	0.28	2/78	2.57	0.07
3	15/75	21.20	4.49	1/52	2.08	2.08	1/42	2.08	2.08
5	84/262	33.02	3.59	2/73	2.77	0.27	1/62	1.56	1.56
10	69/142	50.43	2.99	NA	0.00	NA	NA	0.00	NA
100	NA	0.00	NA	NA	0.00	NA	NA	0.00	NA

n = fraction of cells that after coming out of competence, go back into this state within two cell cycles, with respect to all competence events; NA, not applicable, cells do not reinitiate competence; wt, wild type.

Table S6. Reaction rate values

Reaction rate	Value
k_1	$6.25{\cdot}10^{-5}s^{-1}$
k_2	$0.15625\ s^{-1}$
k_3	$0.2\ s^{-1}$
k_4	$0.0\ s^{-1}$
k_5	$0.00025\ s^{-1}$
k_6	$0.2\ s^{-1}$
k_7	$0.005\ s^{-1}$
k_8	$0.0001\ s^{-1}$
k_9	$0.005\ s^{-1}$
k_{10}	$0.0001\ s^{-1}$
k_{11}	$1.02{\cdot}10^{-6}\ s^{-1}$
k_{-11}	$0.0005\ s^{-1}$
k_{12}	$0.025\ s^{-1}$
k_{13}	$3.5{\cdot}10^{-6}\ s^{-1}$
k_{-13}	$5{\cdot}10^{-5}\ s^{-1}$
k_{14}	$2{\cdot}10^{-5}\ s^{-1}$
k_k	5,000 molecules
k_s	1,562 molecules